Nuclear Instruments and Methods in Physics Research A 776 (2015) 1–7

Contents lists available at ScienceDirect

Nuclear Instruments and Methods in Physics Research A

journal homepage: www.elsevier.com/locate/nima

# Detecting energy dependent neutron capture distributions in a liquid scintillator

Matthew J.I. Balmer [a,*], Kelum A.A. Gamage [a], Graeme C. Taylor [b]

[a] Department of Engineering, Lancaster University, LA1 4YR, UK
[b] Neutron Metrology Group, National Physical Laboratory, Teddington, TW11 0LW, UK

ARTICLE INFO

*Article history:*
Received 10 October 2014
Accepted 26 November 2014
Available online 12 December 2014

*Keywords:*
MCNP
Dosimetry
Directional neutron survey
Neutron capture
ANN
Pattern recognition

ABSTRACT

A novel technique is being developed to estimate the effective dose of a neutron field based on the distribution of neutron captures in a scintillator. Using Monte Carlo techniques, a number of monoenergetic neutron source energies and locations were modelled and their neutron capture response was recorded. Using back propagation Artificial Neural Networks (ANN) the energy and incident direction of the neutron field was predicted from the distribution of neutron captures within a $^{6}$Li-loaded liquid scintillator. Using this proposed technique, the effective dose of $^{252}$Cf, $^{241}$AmBe and $^{241}$AmLi neutron fields was estimated to within 30% for four perpendicular angles in the horizontal plane. Initial theoretical investigations show that this technique holds some promise for real-time estimation of the effective dose of a neutron field.



## 1. Introduction

The radiation protection quantity *effective dose* can be used to provide an estimation of the health risk due to exposure to a neutron field [1]. Using this quantity, the risk estimate accounts for both energy and direction of incidence of a neutron field. Using conversion coefficients, a neutron fluence can be transformed into an effective dose for a given incidence of the neutron field, by applying fluence to effective dose conversion coefficients that change with energy and angle [1]. Fig. 1 shows how the effective dose coefficients change for antero-posterior (AP), postero-anterior (PA), left-lateral (LLAT) and right-lateral (RLAT) incident radiation. It can be seen that the greatest health risk is experienced with the AP direction of incidence, while the lowest risk is with RLAT incidence. Existing neutron survey techniques measure the isotropic dose quantity, *ambient dose equivalent H*(10)*. This dose quantity is used for neutron surveys as it is designed to account for the worst case of the health risk. Although effective dose cannot be measured, previous research has discussed the possibility of using instrumentation to *estimate* effective dose in real-time [2] to understand the human health risk accounting for the anisotropic nature of a neutron field.

A proof of concept for an instrument consisting of a boron-loaded spherical scintillator of 20.32 cm diameter interrogated by multiple photomultiplier tubes (PMTs) has already been undertaken [2]. When a neutron interacts in a liquid scintillator it will undergo a number of elastic collisions. These elastic collisions can be detected by the particle recoil from the collision, causing scintillation of photons proportional to the energy lost to the recoiling particle. If a neutron loses enough energy in the scintillator through these collisions, it is likely that it will be captured, if a high neutron capture cross-section element is present in the scintillator. The energy from this capture reaction remains constant for a given loading element, therefore the light production for a neutron capture remains constant.

By interrogating the scintillator with a number of PMTs, differing numbers of photons will be detected depending on the location of the neutron capture event in the scintillator. By making the interior of the scintillator non-reflective it is thought that the detection of these differences will become easier. This novel concept is shown in Fig. 2. Six photomultiplier tubes are shown, placed equidistantly around the perimeter of the spherical scintillator.

Using Monte Carlo simulation techniques, the location of a large number of neutron capture events within the scintillator was recorded. A pattern relating to energy and direction of incidence of the neutron field to the detector was observed. An example of the neutron capture distribution's dependency on energy can be seen in Fig. 3. It can clearly be seen that differing energies of neutron source exhibit a different pattern of distribution of neutron capture within the scintillator. An artificial neural network was trained with data obtained through Monte Carlo simulations and in this proof-of-concept it was shown that an estimate of effective dose could be achieved using this instrument. However no

* Corresponding author.
*E-mail address:* m.balmer@lancaster.ac.uk (M.J.I. Balmer).

http://dx.doi.org/10.1016/j.nima.2014.11.093
0168-9002/

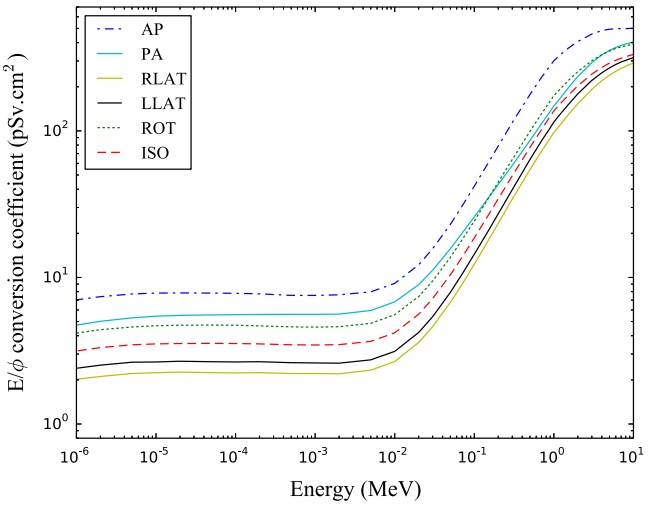


**Fig. 1.** Effective dose coefficients for AP, PA, RLAT, LLAT, ROT (rotational) and ISO (isotropic) are shown. The coefficients used were taken from the latest ICRP recommendations [1].

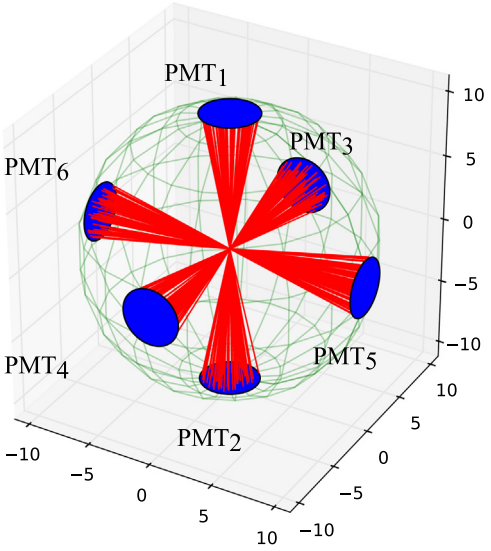


**Fig. 2.** Scintillation from a neutron capture in the spherical scintillator described in this work. The six PMTs shown detect different amounts of light depending on the location of the neutron capture in the scintillator. The interior of the scintillator is coated with a non-reflective coating, so photons which do not hit a PMT are absorbed.

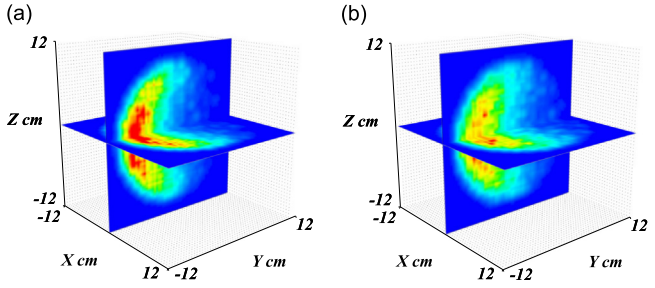


**Fig. 3.** Distribution of neutron captures within a 10.8 cm radius $^{6}$Li-loaded scintillator exposed to two different mono-energetic neutron energies, (a) 10 keV and (b) 100 keV, plots drawn using the Mayavi software library [5].

investigation was undertaken to detect the locality of the neutron capture in the scintillator.

Initial investigations into the design of a novel technique to detect the pattern of neutron capture has been undertaken [3]. This research investigated a suitable scintillator for use in this work, focusing on gadolinium, lithium and boron loaded liquid scintillators. The most promising of the detectors considered was a $^{6}$Li-loaded liquid scintillator.

$$^{1}n + {}^{6}\mathrm{Li} -> t(2.73\ \mathrm{MeV}) + \alpha(2.05\ \mathrm{MeV}) \quad (1)$$

As shown in Eq. (1), two light particles are emitted as a result of neutron capture. These ionising particles deposit their energy close to the capture location within the scintillator. These light particles mean that less quenching of the scintillation will occur when compared to the light yield of a boron loaded liquid scintillator. It is also of note that there is no $\gamma$ emission from the lithium neutron capture reaction. Therefore all products of the capture reaction can be considered useful signals.

Previous investigations into $^{6}$Li-loaded scintillators have shown the detected capture signal to be around 470 keVee (*electron equivalent*) [4]. However, the design of the detector proposed in the scope of this research is such that only a fraction of this light will be collected. It is anticipated that the interior of the detector would be non-reflective and so considering six PMTs of 2.5 cm radius, located equidistantly around the perimeter of a 10.8 cm radius detector (as shown in Fig. 2) only eight percent of the light will be detected for a scintillation event at the centre of the scintillator. This equates to a detected signal of 44 keVee. The anticipated low light level collection will hinder the ability to discriminate desired detection events (neutron captures), from $\gamma$ and proton recoil interactions in the scintillator. It is therefore of interest to investigate a smaller sized scintillator to maximise light collection for Pulse Shape Discrimination (PSD).

This paper looks at the design of a novel method to translate a number of neutron captures in a scintillator into an effective dose. Two sizes of scintillators were investigated, 7.5 cm and 10.8 cm. The larger size was chosen as it was the original proposed size, similar to that of existing neutron survey instruments. The smaller 7.5 cm was chosen for the improved light collection from neutron capture. The ability to determine neutron source energy and incidence are investigated, as well as the effective dose for PA, AP, LLAT and RLAT incident radiation.

## 2. Methodology

Early investigations into the design of this instrument attempted to localise every individual neutron capture event. However, no satisfactory method was found to localise individual neutron captures. These investigations did however provide the basis for the novel method proposed in this paper. This research investigates the potential for utilising the different light level distributions recorded by each PMT for a number of neutron capture events in a scintillator without attempting to reconstruct the capture locations. In this work, 100,000 neutron capture events were investigated for each neutron source energy and location. The method holds promise to be robust with regard to noise on each individual scintillation pulse by collecting a large number of neutron capture events. This simple approach also lends itself well to deployment into a portable real-time system using a field programmable gate array (FPGA) to carry out the processing. This approach is shown in Fig. 4.

### 2.1. Monte Carlo simulation parameters

For investigation of a large number of neutron source energies the Monte Carlo radiation transport code package, MCNP v5.0, was used to simulate neutron capture within a $^{6}$Li-loaded scintillator [6]. The composition of the scintillator is shown in Table 1. Previous simulations using MCNP to investigate neutron capture location in a scintillator have been shown to be in agreement with

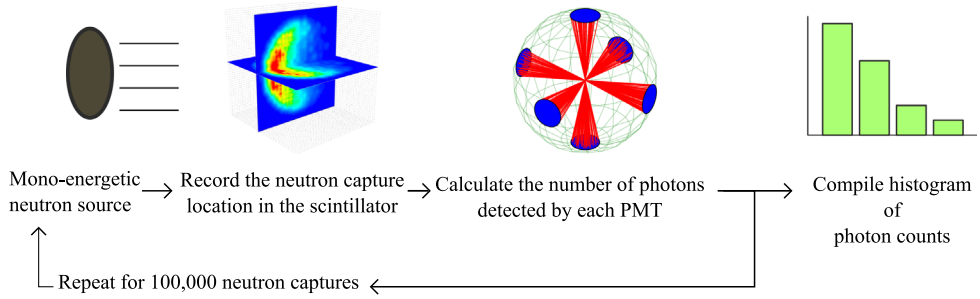


**Fig. 4.** System level schematic diagram of the simulations undertaken. Using Monte Carlo simulation tools, a mono-energetic neutron source emitted a neutron towards the scintillator, if this neutron was captured, the light detected by each PMT was estimated. This was repeated for multiple capture events to build a directional, energy dependent response.

**Table 1**
Fractional mass composition of a typical $^{6}$Li-loaded liquid scintillator of density 0.92 g/cm$^3$.

| Element | C | H | O | N | $^{6}$Li |
|---|---|---|---|---|---|
| Fractional mass | 0.858 | 0.105 | 0.0304 | 0.0026 | 0.004 |

the results obtained using a second simulation package, Geant4 [7,8,3].

In MCNP materials were simulated using the ENDF/B-VII.0 neutron cross-section tables at temperature 293.13 K. To handle low energy thermal scattering of neutrons below 5 eV, MCNP has thermal treatment for hydrogen in polyethylene. For s(α, β) thermal treatment, *poly.01t* was included in the MCNP input file. Using the particle tracking file (PTRAC), neutron capture events were counted, recording the ($x$, $y$, $z$) location of the neutron capture within the detector. The simulations were run for 100,000 neutron capture events. A planar disc, equal to the radius of the scintillator, was used to simulate 22 mono-energetic neutron sources of differing energy, ranging from 15 keV to 5 MeV. The upper energy range was selected due to the isotropic pattern observed in a scintillator of this size as these energy limits are approached [9], when using a 10.8 cm radius detector. For the same reasons, for the 7.5 cm radius detector an upper energy limit of 1 MeV was set, thereby reducing the number of mono-energetic neutron source energies to 14. For each mono-energetic neutron source energy investigated, the source was rotated around the centre of the scintillator at (0, 0, 0) on a radius of 200 cm, to 28 locations in the 4$\pi$ region around the sphere.

### 2.2. Photon transport simulation

It is approximated that a neutron capture at the centre of the spherical scintillator (at the Cartesian coordinate shown in Eq. (2)) will yield 470 keVee of light.

$$(x_{capture}, y_{capture}, z_{capture}) = (0, 0, 0) \tag{2}$$

This light yield is approximated to 1200 photons, which are spread isotropically from the cartesian coordinate as shown in Eq. (2). After travelling distance $r$, each photon will either be absorbed in the non-reflective coating on the interior of the scintillator housing, or detected by a PMT, at spherical coordinate ($\theta$, $\phi$ and $r$). The azimuthal angle is denoted by $\theta$ and the polar angle $\phi$, for example, for PA incidence the spherical angles are ($\pi$, 0). To specify the isotropic spreading of these photons over the 4$\pi$ surface of the sphere, 1200 equidistant points were created. This was achieved using a probability density function sampling $\theta$ and $\phi$ over the ranges [0, 2$\pi$] and [0, $\pi$] respectively. Each of these $n$ locations were then be found using following equations:

$$x_n = r\sin\theta\cos\phi \tag{3}$$

$$y_n = r\sin\theta\sin\phi \tag{4}$$

$$z_n = r\cos\theta \tag{5}$$

Consider a PMT at the coordinate given in Eq. (6). This PMT is located on the plane described by Eq. (7) described by the arbitrary coefficients *(a,b,c)*.

$$(x_{pmt}, y_{pmt}, z_{pmt}) \tag{6}$$

$$ax + by + cz + d = 0 \tag{7}$$

The point of intersection of the photon trajectory with the plane occurs at the coordinates given in Eqs. (8)–(10), where $t$ is an arbitrary variable.

$$x_{intersect} = x_{capture} + (t(x_n - x_{capture})) \tag{8}$$

$$y_{intersect} = y_{capture} + (t(y_n - y_{capture})) \tag{9}$$

$$z_{intersect} = z_{capture} + (t(z_n - z_{capture})) \tag{10}$$

By solving the simultaneous Eqs. (8)–(10), $t$ is found. The distance between the point of the photon trajectory intersection with the plane and the PMT location is calculated. If the distance is less than the radius of the PMT viewing window, this is recorded as a detected photon. The quantum efficiency of the PMT is assumed to be accounted for in the photon yield estimation.

The algorithm described above was implemented using a custom written C program. This algorithm was automated to record the number of photons detected by a given number of PMTs for a given location of scintillation event within the spherical detector. For the investigations in this work a PMT radius of 2.2 cm was chosen. It is assumed that the PMT is directly coupled to the scintillator and no light guide is used.

The number of photons detected by each PMT was normalised to half the photon yield, as this is the theoretical maximum number of photons that can be detected by each PMT (given a capture infinitessimally close to the PMT). The frequency distribution of this normalised photon count was then placed into 8 data bins of 0.01 (20 photons) intervals, the 9th data bin covered 0.09 to 1.0. It was felt that in the detection region of less than 20 photons for a single PMT could be problematic during experimental situations. For this reason the data bin covering 0 to 0.01 was also omitted.

Fig. 3(b) visualised 100,000 neutron captures for a 100 keV mono-energetic source the number of photons detected by each PMT for this simulation is shown in Fig. 5. It can be seen that there is a large difference between PMT$_3$ and PMT$_4$ therefore it can be assumed that a large number of neutron captures occurred closer to PMT$_4$ than PMT$_3$. Inspection of PMT$_5$ and PMT$_6$ shows similar

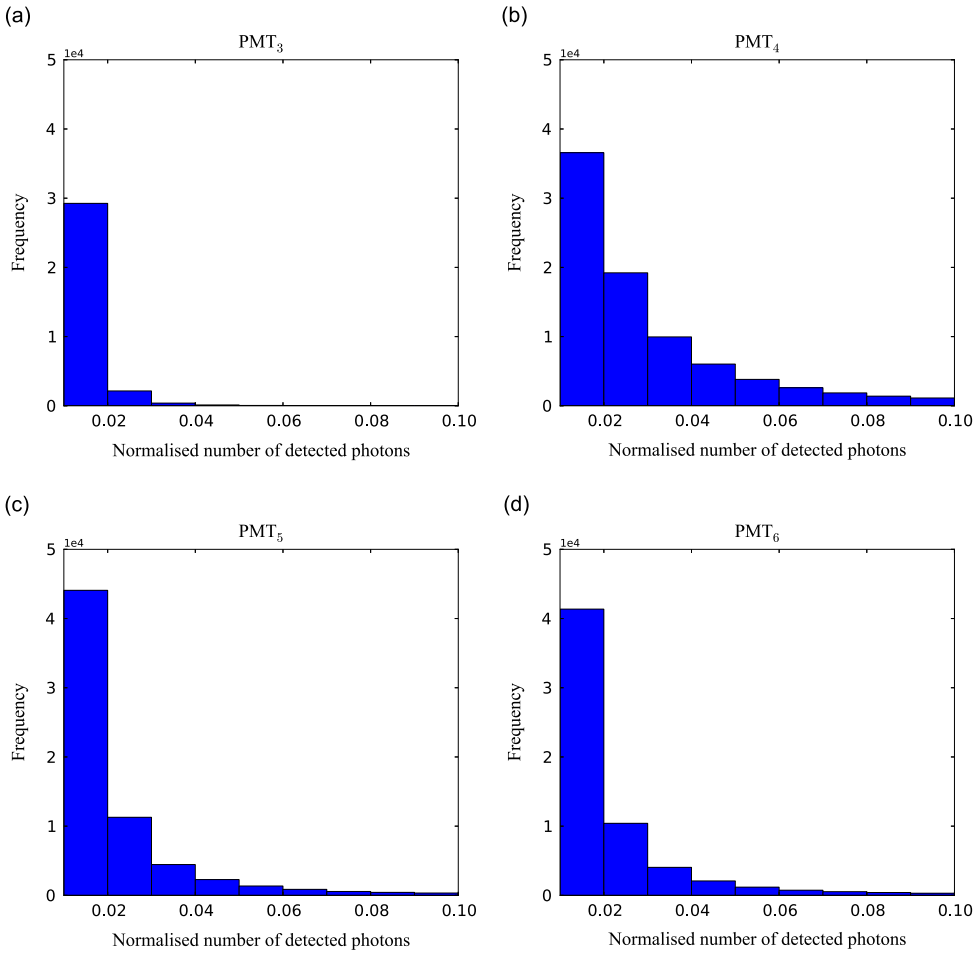


**Fig. 5.** Histogram of the number of photons detected by each PMT. It can be seen that $PMT_5$, $PMT_6$ show similar numbers of photons detected by each PMT. Examining the area of the detector furthest from the neutron source $PMT_3$, exhibits the lowest count. Although $PMT_1$ and $PMT_2$ are not shown, the histograms are similar to those of $PMT_5$, $PMT_6$.

number of photons detected by each PMT respectively. From this information, the direction of incidence of the neutron field can be correlated to the number of photons counted by each PMT.

## 3. Artificial neural network approach

Artificial neural networks (ANNs) are well proven for their abilities in pattern recognition systems. Once a neural network has been trained, the trained network can be deployed into a fast real-time system. Given the benefits of an ANN it was decided to use the C based software library FANN, version 2.2.0 for the investigations in this work [10].

For complicated pattern recognition in multiple dimensions, the back propagation neural network is the most widely applied neural network technique [11]. The network is flexible and can be adapted to different situations by changing the network configuration. Learning coefficients, number of layers, number of neurons and activation functions can all be changed for a given set of input data to optimise the learning of the pattern. Early investigations using an ANN to predict both energy and direction with the same network were found to less successful than two separate ANNs for this purpose. The two networks estimated neutron source energy and neutron incidence respectively. The architecture of the network used in this work for estimating the direction of incidences is shown in Fig. 6. Each network was trained with the same input data. This consisted of 9 discrete bins of the number of

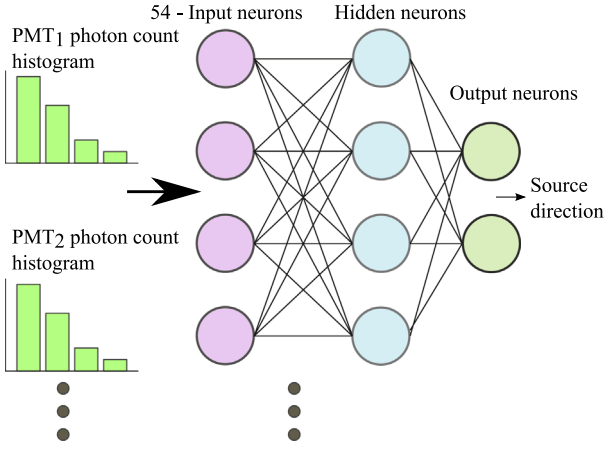


**Fig. 6.** Schematic of the back propagation ANN used in this research to estimate the incidence of neutron field to the detector.

photons detected by each of the PMTs resulting in 54 input neurons for the six PMTs, feeding into 3 layers of neurons with a sigmoid activation function.

The networks trained with an upper energy cut off of 1 MeV, were trained with 196 facts (7 mono-energetic neutron sources, ranging from 15 keV to 1 MeV located at 28 locations around the spherical scintillator). The networks trained with an upper energy cut off of 5 MeV were trained with 336 facts (12 mono-energetic

neutron sources, ranging from 15 keV to 5 MeV located at 28 locations around the spherical scintillator). The resilient propagation (RPROP) training algorithm was used for each network [12].

All data used in the network was normalised between 0 and 1. The spherical angle $\phi$ was normalised over the range 0, $\pi$ and $\theta$ over the range 0, $2\pi$. The mean squared error (MSE) used to evaluate network convergence is the error of these normalised values.

Previous research has shown that between 1 and 10 MeV in a 10.8 cm radius scintillator, visually, the anisotropic pattern of capture can no longer be seen [9]. By reducing the size of the scintillator further to 7.5 cm radius, the light collected from each capture will increase (from around 9% to 17%). However it is expected that this reduction will further impede the detection abilities of the scintillator in the upper energy ranges. Two different scintillator radii were considered in this work, 7.5 cm and the original radius of 10.8 cm. Another consideration with the radius of the detector was the additional mass the larger detector will further impede portability of this instrument. A reduction in size from 10.8 cm to 7.5 cm reduces the mass from around 4.7 kg to 1.6 kg (not accounting for the instrumentation electronics). It was noted during the initial investigations of the 7.5 cm detector that no satisfactory results could be obtained when training the network with an upper energy limit of 5 MeV. By reducing this to 1 MeV, the network was observed to converge below the desired MSE.

Each network investigated was optimised in terms of numbers of hidden neurons. Starting with 10 hidden neurons it was observed that the network convergence was above the MSE. Increments of 5 neurons were added to the network, and retraining was undertaken. More hidden neurons were added to the network until the point of convergence for the MSE error on the network was below that of the prescribed MSE training cut off. This MSE value was obtained experimentally by ensuring that the error on the training data was suitably low, but not low enough that the network over trained on the training facts and became less flexible to testing facts it had never seen before. The final configurations of the ANNs are shown in Table 2.

The instruments ability to work with data it has not received training for is a crucial requirement of this instrument. Once trained, each network was tested with a data set interpolating between neutron source energies and directions found in the training data. Training a network with a large number of neutron sources in a laboratory environment would be a time consuming task, so the network's abilities to interpolate between training facts should reduce the need for a large number of training facts.

## 4. Results

### 4.1. Monoenergetic neutron sources

To assess the suitability of the training of the ANNs, each network was tested with monoenergetic neutron source energies interpolating between the training energies. Four source locations were selected that were not found in the data set. In each of these cases the neutron field located at directions AP, PA, RLAT and LLAT to the detector.

For validating the training of the direction ANN, the spread of the estimated angles were plotted and this is shown in Fig. 7a and b. Each data cluster represents a single source location and within that cluster, each data point is one of the monoenergetic neutron source energies. It can be seen from Fig. 7a and b that for monoenergetic neutrons, both detectors can resolve the azimuthal angle $\theta$ reasonably well. However it can be seen that with the estimation of the polar angle component, $\phi$ there is a spread of around 45°in this estimation for the 7.5 cm detector. For the 10.8 cm this worsens to a spread of around 63°.

It is thought that at energies greater than 1 MeV the isotropic pattern of capture makes it hard to resolve the direction of neutron incidence. For each energy, the network is trained with 24 different source locations. So in the range of 1–5 MeV the network is potentially seeing around 100 facts that all appear similar to the network, in terms of input values. With noise propagated into this data it is thought that this matter will only become worse.

To investigate the validity of the ANN estimating energy, each the ANN estimation energy was plotted against the known value of each monoenergetic neutron source energy. This can be seen in Fig. 8a and b, with four points in each data cluster representing each source location. It can be seen that the 7.5 cm detector is able to estimate the energy much better than the 10.8 cm detector at lower neutron energies.

### 4.2. Testing the ANN with a distributed neutron field

With the promising results obtained modelling monoenergetic neutron sources it was decided to investigate if the ANN could estimate the effective dose of a more complex neutron fluence with energy dependency. For these investigations three radionuclide source were investigated; $^{252}$Cf, $^{241}$AmBe and $^{241}$AmLi. The neutron spectra from these three sources can be seen in Fig. 9. Due to the higher energies found within these fields, only the 10.8 cm detector trained up to 5 MeV was used. The neutron energies found within these spectra are both above and below those used in the training data. The source was located AP, PA, RLAT and LLAT to the detector. No further training was undertaken with the networks from those used for monoenergetic tests.

The results shown in Table 3 show promising results of the estimation of the effective dose from these distributed fields. The maximum error on the estimation of the effective dose was found to be 30%. With the $^{241}$AmBe source it can be seen in Fig. 9 that there is a contributing fluence of neutrons above the upper ANN monoenergetic training energy of 5 MeV. With neutrons above those found in the training energies contributing to the spectra the ANN is able to estimate this effective dose to within 20%. The broader distribution of the $^{241}$AmLi can be seen to estimate the dose with a slightly larger error compared to the $^{252}$Cf and $^{241}$AmBe results. It is thought that the lower energies found within this spectra could be causing this higher error as it can be seen in Fig. 8b that ANN is not able to estimate these lower energies as accurately.

**Table 2**
Configuration parameters of the six ANNs investigated in this work.

| Scintillator radius (cm) | ANN output | Hidden neurons | Normalised MSE cut off ($10^{-4}$) | Training energy range |
|---|---|---|---|---|
| 7.5 | Energy | 50 | 6 | 10 kev–1 MeV |
| 7.5 | Direction | 30 | 6 | 10 kev–1 MeV |
| 10.8 | Energy | 54 | 2 | 10 keV–5 MeV |
| 10.8 | Direction | 28 | 6 | 10 keV–5 MeV |

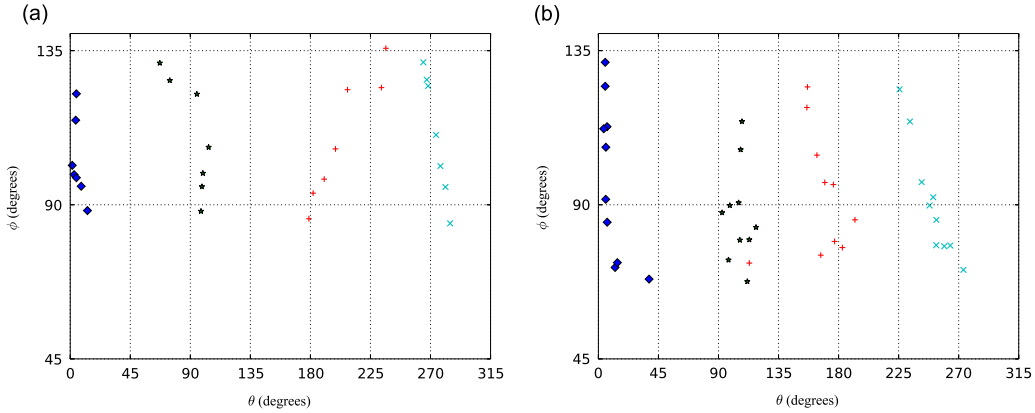


**Fig. 7.** ANN estimation of the incidence of a monoenergetic neutron field for four different source locations (AP (0°), PA (180°), RLAT (90°) and LLAT (270°)) for (a) 7.5 cm detector and (b) 10.8 cm detector.

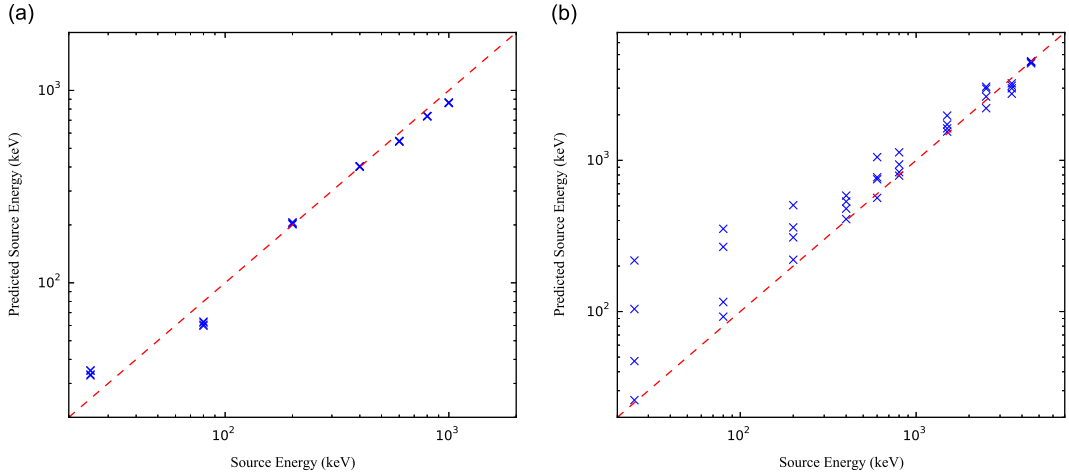


**Fig. 8.** ANN estimation of the energy of a monoenergetic neutron field compared against the known energy of this field. Each energy was repeated for four different source locations (AP, PA, RLAT and LLAT) with the two detectors of radius (a) 7.5 cm and (b) 10.8 cm.

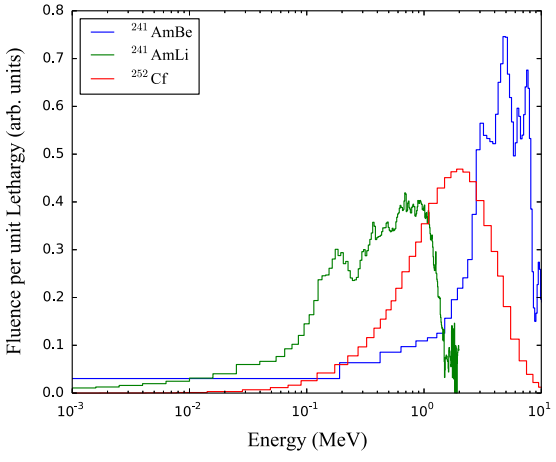


**Fig. 9.** The neutron spectra of three distributed fields used for testing the ANN in this work; $^{252}$Cf, $^{241}$AmBe and $^{241}$AmLi.

**Table 3**
ANN estimate of effective dose of 3 radionuclide neutron sources investigated in this work.

| Neutron source | Neutron incidence | Calculated effective dose (pSv cm$^2$) | ANN estimated effective dose (pSv cm$^2$) | Error of estimated effective dose (%) |
|---|---|---|---|---|
| $^{252}$Cf | AP | 350 | 392 | 11 |
| | PA | 209 | 196 | 6 |
| | RLAT | 138 | 107 | 26 |
| | LLAT | 159 | 136 | 15 |
| $^{241}$AmBe | AP | 426 | 421 | 1 |
| | PA | 291 | 238 | 20 |
| | RLAT | 197 | 168 | 16 |
| | LLAT | 222 | 182 | 20 |
| $^{241}$AmLi | AP | 152 | 207 | 30 |
| | PA | 77 | 87 | 13 |
| | RLAT | 48 | 35 | 32 |
| | LLAT | 57 | 43 | 28 |

## 5. Conclusion

In this work it has been investigated using Monte Carlo simulations if the effective dose of a neutron field could be estimated based upon the pulse height spectra from a number of neutron captures in a scintillator. The results obtained showed promise. Each ANN was optimised with extensive training and these optimal networks were then validated with data that the ANN had not seen during training. This consisted of monoenergetic neutron source energies interpolating between the training energies and different source locations. The network was able to resolve the azimuthal angle of incidence reasonably well. However the polar angle of incidence was found to have a large spread. It is not known that how much this would affect the effective dose as with the current ICRP fluence to effective dose conversion coefficients no values are published to account for these polar angles. Further investigation will be required to quantify this.

Following initially promising results with the monoenergetic neutron fields, the networks were then tested with three neutron sources. These sources were located AP, PA, RLAT, LLAT, locations not found in the training data. The ANN was able to estimate the effective dose with an accuracy of 30% or less.

Reducing the detector size to 7.5 cm radius, an upper limit of 1 MeV is imposed. However with the larger radius detector less light will be collected from each neutron capture event. This will likely impede the abilities of the detector to discriminate a scintillation as a neutron capture. This capture detection ability is crucial for the instrument. For the use of the instrument in the upper energy ranges it is thought that a polyethylene moderator could be installed around the detector. Whilst adding mass to the instrument this would potentially enable a energy and direction of the field to be resolved at energies above 1 MeV. This would not reduce on the amount of light collected by each neutron capture, and thus not impede the ability to perform PSD on the detected light pulses.

To realise this instrument into one which can be used to estimate the effective dose of a broader distributed workplace fields further investigation is required. Specifically, to see if the ANN can cope with multiple angles of incidence and broad energy distributions with stronger thermal components. It is anticipated that the proton recoil distribution could be investigated to aid the ANN in these more broad energy spectra. For complex fields with multiple incidence it needs to be investigated that how much training the ANN would require to deal with multiple unknown angles of incidence.

## Acknowledgements

The authors would like to acknowledge the funding support from EPSRC and National Physical Laboratory, Teddington, UK. The authors acknowledge the use of the package Matplotlib for plots drawn in this research [13].

## References

[1] N. Petoussi-Henss, W.E. Bolch, K.F. Eckerman, A. Endo, N. Hertel, J. Hunt, M. Pelliccioni, H. Schlattl, M. Zankl, Annals of the ICRP 40 (2) (2010) 1.
[2] G.C. Taylor, Radiation Measurements 45 (10) (2010) 1301. http://dx.doi.org/10.1016/j.radmeas.2010.08.019.
[3] M.J.I. Balmer, K.A.A. Gamage, G.C. Taylor, Journal of Instrumentation 9 (01) (2014) P01007. http://dx.doi.org/10.1088/1748-0221/9/01/P01007.
[4] C. Bass, E. Beise, H. Breuer, C. Heimbach, T. Langford, J. Nico, Applied Radiation and Isotopes 77 (2013) 130. http://dx.doi.org/10.1016/j.apradiso.2013.03.053.
[5] P. Ramachandran, G. Varoquaux, Computing in Science and Engineering 13 (2) (2011) 40.
[6] A General Monte Carlo n-Particle Transport Code, Version 5.
[7] S. Agostinelli, et al., Nuclear Instruments and Methods in Physics Research Section A: Accelerators, Spectrometers, Detectors and Associated Equipment 506 (3) (2003) 250. http://dx.doi.org/10.1016/S0168-9002(03)01368-8.
[8] J. Allison, et al., IEEE Transactions on Nuclear Science NS-53 (1) (2006) 270. http://dx.doi.org/10.1109/TNS.2006.869826.
[9] M.J. Balmer, K.A. Gamage, G.C. Taylor, Nuclear Instruments and Methods in Physics Research Section A: Accelerators, Spectrometers, Detectors and Associated Equipment 735 (2014) 7. http://dx.doi.org/10.1016/j.nima.2013.08.087.
[10] S. Nissen, Implementation of a Fast Artificial Neural Network Library (FANN) (2003).⟨http://fann.sf.net⟩.
[11] R. Hecht-Nielsen, Theory of the backpropagation neural network, in: International Joint Conference on Neural Networks, 1989, IJCNN, IEEE, 1989, p. 593–605.
[12] M. Riedmiller, H. Braun, A direct adaptive method for faster backpropagation learning: the RPROP algorithm, in: IEEE International Conference on Neural Networks, 1993, IEEE, 1993, p. 586–591.
[13] J.D. Hunter, Computing in Science and Engineering 9 (3) (2007) 90.